ACS Catalysis

Article

Cobalt encapsulated in N-doped graphene layers: an efficient and stable catalyst for hydrogenation of quinoline compounds

Zhongzhe Wei, Yiqing Chen, Jing Wang, Diefeng Su, Minghui Tang, Shanjun Mao, and Yong Wang

ACS Catal., **Just Accepted Manuscript** • DOI: 10.1021/acscatal.6b01240 • Publication Date (Web): 26 Jul 2016

ACS Publications

ACS Catalysis is published by the American Chemical Society. 1155 Sixteenth Street N.W., Washington, DC 20036

Cobalt encapsulated in *N*-doped graphene layers: an efficient and stable catalyst for hydrogenation of quinoline compounds

*Zhongzhe Wei, Yiqing Chen, Jing Wang, Diefeng Su, Minghui Tang, Shanjun Mao, Yong Wang**

Advanced Materials and Catalysis Group, ZJU-NHU United R&D Center, Department of Chemistry, Zhejiang University, Hangzhou 310028, P. R. China.

ABSTRACT: Porous nitrogen-doped graphene layers encapsulating cobalt nanoparticles (NPs) were prepared by the direct pyrolysis process. The resulting hybrids catalyze the hydrogenation of diverse quinoline compounds to access the corresponding tetrahydroderivatives (THQs), important molecules present in fine and bulk chemicals. Near quantitative yield of the corresponding THQs were obtained under optimized conditions. Notably, various useful substituted quinolines and other biologically important *N*-heteroarenes are also viable. The enhanced stability of the catalyst is ascribed to the encapsulation structure, which can enormously reduce the leaching of base metals and protect metal NPs from growing larger. The achieved success in the encapsulation of metal NPs within graphene layers opens up an avenue to design highly active and reusable heterogeneous catalysts for more challenging molecules.

KEYWORDS: encapsulated structure; chemoselective hydrogenation; metallic cobalt; *N*-doped graphene layers; quinoline

INTRODUCTION

Catalysts, especially metallic catalysts, play a dominate role in industrial applications. The reusability of catalysts is an important issue in green chemistry and ecological economics.[1] In this respect, development of catalysts using base metals, including Fe[2,3], Co[4-6] and Ni[7,8], is prevailing for their distinct electronic structures[9] and magnetic property. Especially, the specific advantage of magnetic nanomaterials is that they can be effectively recovered by an external magnetic field (typically >99%).[10] However, magnetic NPs tend to aggregate when treated without any protection agents, thus losing their unique properties derived from their small size.[10] For another, leaching of earth-abundant metals (e.g., Co) may also occur, which is prone to irreversible deactivation.[11] Therefore, the rational design of stable nano-magnetic materials based on earth-abundant metals is challenging and attractive.

1,2,3,4-Tetrahydroquinoline (py-THQ) and its derivatives are important building blocks in pharmaceuticals, agrochemicals, and various fine products.[12,13] The general synthesis method is the direct hydrogenation of quinolines, which is the most convenient and hopeful way due to the high atom efficiency.[13,14] However, quinoline hydrogenation ideally involves the possibility that py-THQ, 5,6,7,8-tetrahydroquinoline (bz-THQ) and decahydroquinoline (DHQ) may produce in the reaction networks (Scheme 1). To achieve the chemoselective hydrogenation of pyridine ring without byproducts remains a challenge task. Many homogeneous metal catalysts, such as Rh[15,16], Ir[17,18] and Ru[19] have been applied in the transformation. Despite the high activity and selectivity, the difficulties in recovering the catalysts, ligand, and additives from the reaction mixtures limit the catalysts on industrial scale. Up to now, a series of novel heterogeneous catalytic system using precious metal catalysts, including Au,[20-22] Pd,[12,13,23,24] Pt,[25] Ru[26-30], Ir,[31] Rh[32-34] and multi-metallic catalysts[35] have been developed, but the catalysts based on magnetic metal NPs

are rarely reported.[5,7,8] The problem often arising is that the noble metals are not selective and perform low tolerance for functional groups.[36] Particularly worth mentioning is that the catalysts are difficult to recycle due to the presence of N-heterocycle potentially causing catalyst poisoning through the coordination of nitrogen atoms with the metal NPs.[37,38] To overcome the limitations, the metal NPs encapsulated with porous carbon shell is an impressive strategy.[6,39-41] The major advantages are that (1) the encapsulation structure can elegantly regulate the electronic structure of metal NPs and strictly control the aggregation of NPs;[42-44] (2) the structure can stabilize the NPs and greatly reduce the leaching of base metals for the catalyst;[39,43] (3) the encapsulation structure can weaken the strong coordination between N-heterocycle and active metal NPs. Accordingly, the life of the catalyst can be prolonged; (4) encapsulation the metal NPs within porous carbon shells ensures that the catalytically active sites are easy to approach and enormously inhibit the mass transfer limitation.[39] Herein, we design the nano-magnetic material featuring of nitrogen-doped carbon-coated cobalt NPs and further apply the catalysts in hydrogenation of N-heteroarenes compounds. The hybrids serve as an efficient, selective and robust catalyst in the transformation. Interestingly, the substrates can be smoothly converted into the products without using commercial magnetic stirring bars due to the good magnetic response of the catalyst.

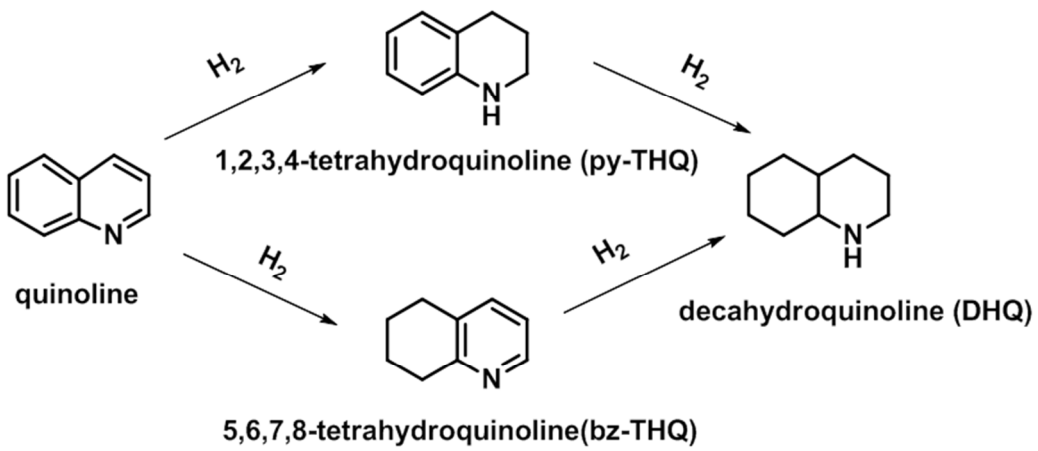

Scheme 1. Possible reaction pathways for quinolone hydrogenation

RESULTS AND DISCUSSION

The hybrids (denoted as CoO_x@CN) were obtained in one step through pyrolysis of D-glucosamine hydrochloride (GAH), cobalt acetate, and melamine at 800 °C. At temperature above 450 °C, melamine gradually condensed to generate graphitic carbon nitride (g-C_3N_4), acting as soft template. Meanwhile, carbon sheets formed on the interlayer of g-C_3N_4 through the self-polymerization of GAH. The cobalt-based NPs were confined between the g-C_3N_4 and carbon sheets. Then, g-C_3N_4 is fully decomposed at higher temperature and the carbon sheets on the interlayer of the g-C_3N_4 were maintained.[45] Finally, cobalt-based NPs were encapsulated into the N-doped carbon sheets and produced the catalysts.[46,47].

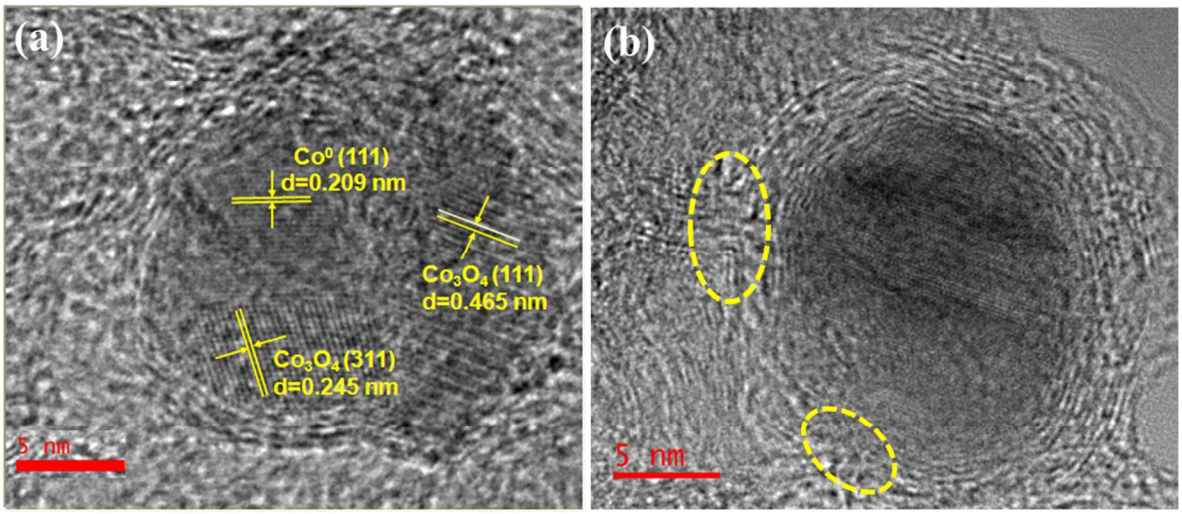

Figure 1. Representative HRTEM images of CoO_x@CN.

High-solutiontransmission electron microscopy (HRTEM) was used to investigate the morphology and structure of CoO_x@CN. It is observed that Co NPs are well encapsulated inside the carbon layers (Figure1,S1). It is worth to note that obvious defects like small channels can be observed on the surrounded carbon layers as demonstrated in Figure 1b, where the reaction may occur. An obvious hysteresis loop occurred in N_2 adsorption–desorption isotherm, which is the characteristic of mesopores (Figure S2). The application of the BET model resulted in the surface area of 531 $m^2 g^{-1}$. The distribution of pore size calculated by the BJH method is around 12 nm (Figure S2). The large surface area and the mesoporous pores ensure that the substrates access the active sites easily without suffering from high mass transfer causing by the carbon shells. HRTEM, X-ray diffraction (XRD) and X-ray photoelectron spectroscopy (XPS) (Figure S3-5) show that *in situ* generated Co^0, Co_3O_4, and nitrogen-doped carbon shells together constitute CoO_x@CN through one-pot synthesis. Interestingly, Co^0 in CoO_x@CN is exceptionally stable. Definite metallic Co reflections were displayed in the XRD pattern for the catalyst after acid treatment (Figure S6), providing the evidence of the enhanced stability of Co^0

with the protection of nitrogen-doped graphene layers. The magnetic properties of CoO_x@CN were measured at 300 K with Physical Property Measurement System (PPMS-9). As shown in Figure 2, CoO_x@CN exhibits a soft ferromagnetic behavior at room temperature. The saturation magnetization (MS) of the catalyst is 22.3 emu/g at 300 K. The catalyst can be readily separated and recycled with a magnet after the reaction due to the magnetic property.

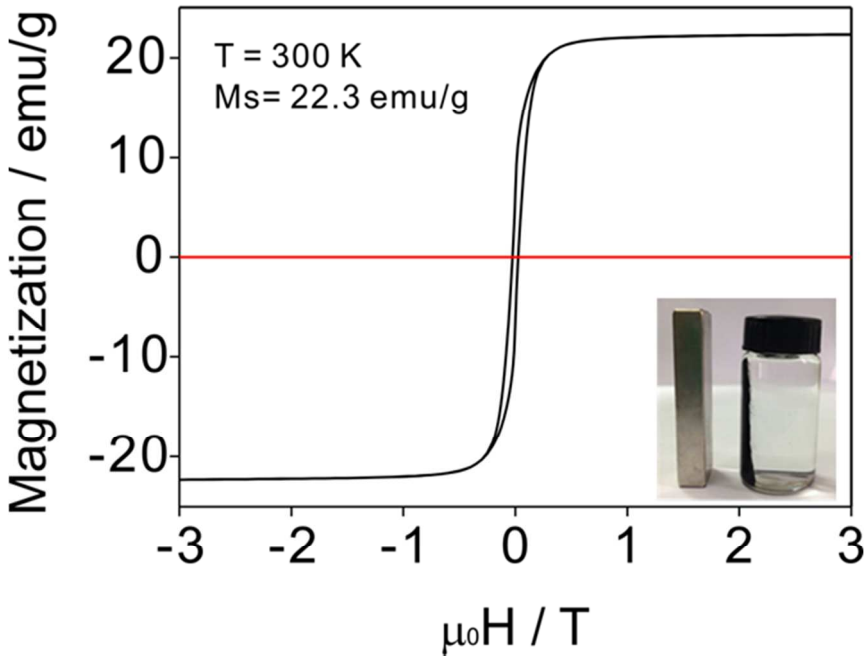

Figure 2. Magnetization data analysis for CoO_x@CN. Inset is the photograph that shows the magnetism of CoO_x@CN.

To exploration the catalytic properties of CoO_x@CN, we select the hydrogenation of the benchmark substrate quinoline as a model reaction. First, the degree of sensitivity of our analytical methods was investigated. We prepared an ethanol solution including possible reduction products including 0.0825 mg/mL DHQ, 0.1225 mg/mL 5,6,7,8-THQ and 0.1625 mg/mL 1,2,3,4-THQ as a sample. From the GC trace (Figure S7), three definitely detectable

peaks at 8.800, 9.861 and 11.225 min are observed, which correspond to DHQ, 5,6,7,8-THQ and 1,2,3,4-THQ, respectively. The results show that the analytical method possesses a high degree of sensitivity. Pleasingly, the evolution of the reactant and product distributions with reaction time revealed that quinoline can be smoothly converted into py-THQ under mild conditions and there was no bz-THQ and DHQ detected in this CoO_x@CN catalytical system (Figure 3). Quantitative yield of py-THQ was obtained in 3 h. CoO_x@CN hydrogenates quinoline with a TOF of 4.1 h^{-1}, which is better than the reported noble metal-free catalysts[5] and even comparable to some noble metal catalysts[15] (Table S3). The high activity and selectivity of CoO_x@CN make it possible in industrial applications. Interestingly, quinoline can also be converted to py-THQ successfully when no commercial magnetic stirring bar used (Figure S8). The tantalizing results suggest that the CoO_x@CN serve as catalytic active sites as well as nanoscale magnetic stirring bars. The reason may come from the magnetic property of CoO_x@CN, which can mix the reactant and contact with the reactant sufficiently under an external magnetic field.[48]

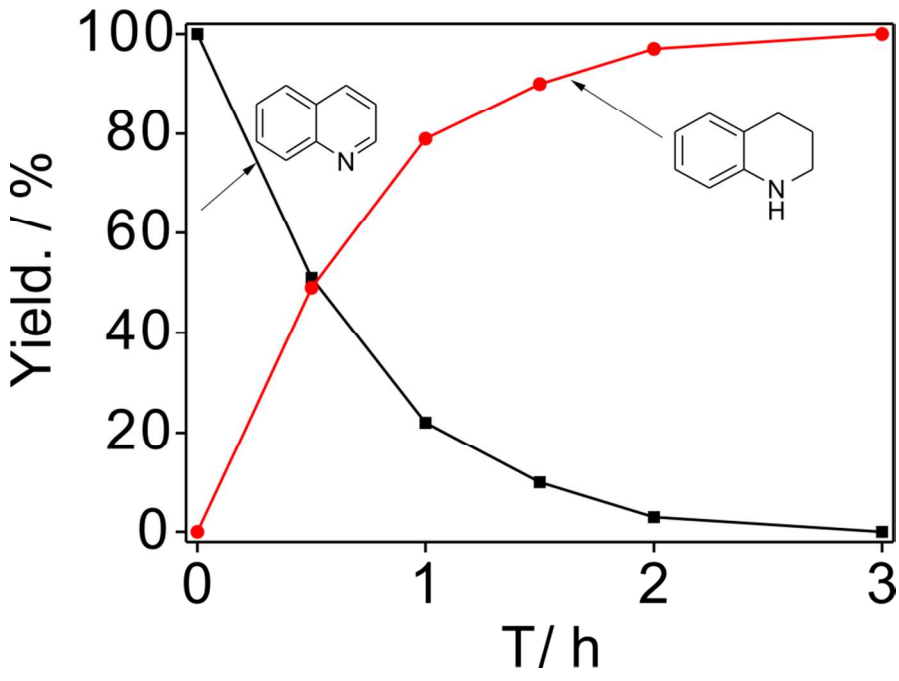

Figure 3. Kinetic curves for quinoline hydrogenation with CoO_x@CN. Reaction conditions: quinoline (0.5 mmol), CoO_x@CN (10mg), CH_3OH (5 mL), 3 MPa H_2, 120 ^oC.

Next, the reaction conditions were optimized for the hydrogenation of quinoline through variation of the solvent, temperature, and pressure. Solvents make difference in heterogeneous catalytic reactions and can influence the activity and selectivity of catalysts. As demonstrated in Table 1, CoO_x@CN promoted the chemoselective hydrogenation of pyridine ring and performed perfect selectivity. In terms of polar and nonpolar reactants, previous studies have been reported that more polar solvents benefit the hydrogenation of less polar substrates. However, the order of the conversion of quinoline in the tested solvents is as follows: methanol > H_2O > ethanol > toluene > DMF > 1,4-dioxane > cyclohexane, which was not consistent with the polarity of solvents. The results were consistent with the hydrogenation of quinoline using Pd@ompg-C_3N_4.[13] It seems that CoO_x@CN performs generally better in protic solvents. For selectivity, we could readily achieve the selectivities toward py-THQ in the range 95-100% in various solvents listed below. To explain the perfect selectivity of CoO_x@CN, Raman tests of the treated catalyst (adsorption with quinoline) and the pristine catalyst were conducted. The interaction between the pyridine ring and the graphene layers was visible in the D- and G-band shift in the Raman spectra, as shown in Figure S9. The downshift by 8 cm^{-1} of treated CoO_x@CN (adsorption with quinoline) with respect to pristine catalyst is evidence of charge transfer from N in pyridine ring to the covered graphene layers in CoO_x@CN[49-51]. The charge transfer suggests the strong interaction between the pyridine ring and the N-doped graphene layers, which favors the production of py-THQ and finally achieves the high selectivity.

Table 1. Effect of solvents on the selective hydrogenation of quinoline using CoO_x@CN [a]

Entry	Solvent	Conv. (%)[b]	Sel. (%)[b]	p[d]
1	Cyclohexane	63	100	0.1
2	Toluene	92	97	2.4
3	1,4-Dioxane	86	95	4.8
4	DMF	86	100	6.4
5	Ethanol	92	99	4.3
6	Water	98	97	10.2
7[c]	Methanol	100	100	6.6

[a]Reaction conditions: quinoline (0.5 mmol), CoO_x@CN (10mg), solvent (5 mL), 3 MPa H_2, 120 °C, 4 h. [b]Conversion (Conv.) and selectivity (Sel.) were determined by GC and GC–MS. [c]3 h. [d] Solvent polarity.

The effects of hydrogen pressure (0.5-3.5 MPa) and temperature (60-120 ^{o}C) were also briefly examined. The conversion of quinoline as a function of the pressure of H_2 is given in Table 2. The results show that conversion steadily increased from 0.5-3 MPa and did not change obviously thereafter. As the H_2 pressure increased, the dissolution of molecular H_2 in the solvent would be promoted, thus obtaining increased TOF value. However, when the surface of the catalyst is mostly covered by dissociated H atoms, the TOF value would not be improved further with the increased H_2 pressure[52]. The catalytic activity of CoO_x@CN is sensitive to the reaction temperature. Reducing the reaction temperature to 100 ^{o}C with 3 MPa H_2, obtained a marked drop in conversion (81%) yet excellent selectivity. Further reducing the temperature to 90°C, both of the conversion and selectivity declined. Similarly, lowering the reaction temperature to 60 ^{o}C afforded an inferior conversion, only furnishing product in 8% yield. For further studies,

we worked at 3 MPa and 120 ^{o}C, as these conditions represented the best compromise between activity and selectivity.

Table 2. The influence of temperature and hydrogen pressure on the hydrogenation of quinoline catalyzed by CoO_x@CN[a]

Entry	T (^{o}C)	P (MPa)	Conv. (%)[b]	Sel. (%)[b]	TOF (h^{-1})
1	60	3	8	100	0.3
2	90	3	74	99	2.7
3	100	3	81	100	2.9
4	120	3	100	100	3.6
5	120	0.5	15	99	0.5
6	120	1	44	99	1.6
7	120	2	70	99	5.1
8[c]	120	3	90	100	6.5
9[c]	120	3.5	91	100	6.6

[a]Reaction conditions: quinoline (0.5 mmol), CoO_x@CN (10mg), solvent (5 mL), 3 h.

[b]Conversion (Conv.) and selectivity (Sel.) were determined by GC and GC–MS. [c]1.5 h.

To further evaluate the catalytic performance, the CoO_x@CN catalyst was compared with FeO_x@CN, NiO_x@CN and several commercial available catalysts including cobalt powder, Co_3O_4, Ru/C, Pd/C and Pt/C in the hydrogenation of 6-chloroquinoline under identical conditions (Table 3). Clearly, CoO_x@CN was the most efficient catalyst, exhibiting fine selectivity toward halo-substituted py-THQ with no appreciable formation of any other side products (Table 3, entry 4). Commercial available Co_3O_4, cobalt powder and CoO_x-AC (CoO_x NPs deposited to the outer surface of active carbon) were not active for the reaction, suggesting the synergistic effect between CoO_x and CN (Table 3, entries 1-3). Despite both of FeO_x@CN and NiO_x@CN can serve as nanosacle magnetic stirring bars due to their magnetic properties, they performed poor activity in the reaction, yielding halo-substituted py-THQ in 1% and 17%, respectively (Table 3, entries 5-6). For Ru/C, Pt/C and Pd/C, the formation of undesirable dehelogenation products obviously occurred. Accordingly, the reaction proceeded unselectively in rather low yield (Table 3, entries 7-9). These results emphasize that CoO_x@CN displayed impressive selectivity in the hydrogenation of quinoline compounds with sensitive substituted groups, much better than the precious metal catalysts.

Table 3. Catalytic results of the hydrogenation of 6-chloroquinoline on various catalysts [a]

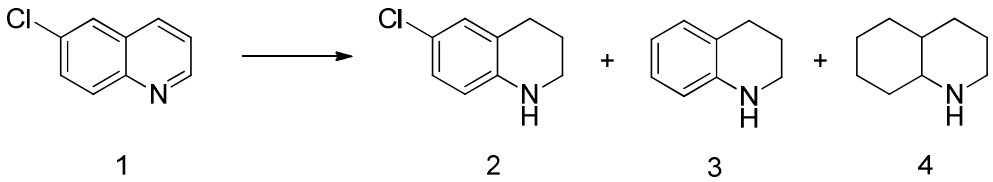

Entry	Catalysts	Conv. [b] (%)	Sel. [b] (%)		
			2	3	4

1	cobalt powder	1	100	-	-
2	Co_3O_4	-	-	-	-
3	CoO_x-AC	6	98	-	-
4	CoO_x@CN	99	97	3	-
5	FeO_x@CN	1	100	-	-
6	NiO_x@CN	18	94	3	3
7	Ru/C[c]	100	16	34	38
8	Pt/C[c]	100	17	30	36
9	Pd/C[c]	100	-	13	62

[a]Reaction conditions: 6-chloroquinoline (0.5 mmol), Catalyst (metal: 9 mol%), CH_3OH (5 mL), 3 MPa H_2, 110 °C, 3 h. [b]Determined by GC and GC–MS. Only the main products are listed. [c]Catalyst (10 mg).

Leaching of active components in the reaction liquid should be taken into consideration, which resulting in the deactivation of catalyst.[53] To shed light on this, we analyzed the cobalt content of the recycled catalyst by ICP-AES. The cobalt content declined slightly to 22.1 wt% from 27.1 wt% after the 12th recycle (Table S2). In an individual experiment, 57 % conversion of quinoline was obtained in 1 h at 120 ^{o}C with 3 MPa hydrogen. Then the reaction was hot filtered by centrifugation to collect the liquid phase. Interestingly, no additional product yield after further

stirring the filtrate in 1 h under the identical conditions above, indicating that the leached cobalt in the liquid did not contribute to the activity.

In terms of the reusability of the catalyst, we performed the selective hydrogenation of quinoline using CoO_x@CN at 120 ^oC and 3 MPa in successive runs and compiled the results in Figure 4a. Some work has revealed that the catalysts used in the hydrogenation of quinoline quickly became inactive due to the strong coordination of nitrogen atoms in quinoline and its hydrogenation products with the metal NPs.[28,29,54] Nevertheless, CoO_x@CN showed a relatively stable performance and could recycle 12 times, which has never been achieved by noble metal-free catalysts. The result indicated that our catalytic system can greatly resist the poison of quinolone and its hydrogenation products.

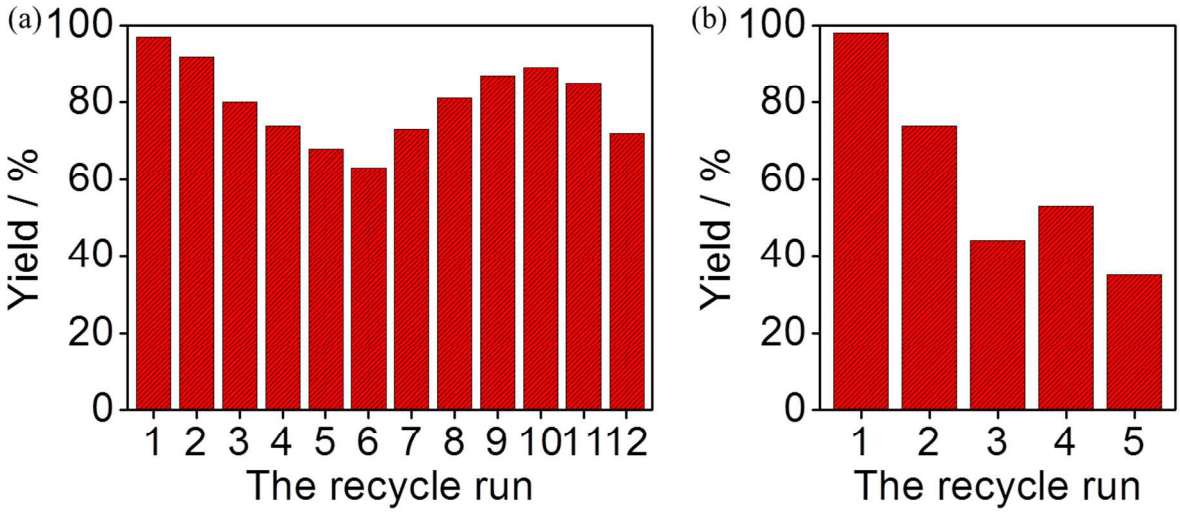

Figure 4. Reuse of CoO_x@CN (a) and CoO_x-CN (b). Reaction conditions: quinoline (1 mmol), Catalyst (20 mg), CH_3OH (10 mL), 120 ^oC, 3 MPa H_2, 3 h for each recycle.

Initially, the yield of py-THQ decreased gradually to 63% after the sixth run. Interestingly, the activity can recover to some extent and the yield steadily increased to 89% after the tenth recycle. Next, CoO_x@CN displayed a slight inactivation in the following recycle experiments,

indeed giving a 57% conversion after the twelfth run. The relatively high activity during the recycle should be attributed to the N-doped graphene layers. To verify the necessity of the encapsulated structure, we prepared the sample CoO_x NPs deposited to the outer surface of CN (denoted as CoO_x-CN) for comparison (see XRD in Figure S10). The CN was obtained according our reported work.[55] CoO_x-CN can also achieve the transformation of quinoline to py-THQ selectively. However, in term of recyclability of the catalyst, the CoO_x-CN exhibited a remarkable inactivation in the process of reuse, furnishing a poor yield (35%) after five times use (Figure 4b). The particle size distribution of the CoO_x@CN after 12 cycles showed that the mean particle size is ~12.8 nm, almost the same with the fresh catalyst (Figure S11). However, for CoO_x-CN, obvious particle aggregation occurred (Figure S12). More importantly, the cobalt content declined slightly for CoO_x@CN, approximately 2% Co leaching for a recycle in average. Notably, the cobalt content of the CoO_x-CN fell sharply to 16.7 wt% from 25.5 wt% in the fifth reuse, approximately 10% Co leaching for a recycle in average (Table S2). Such significant difference between CoO_x@CN and CoO_x-CN was ascribed to the versatile encapsulated structure. On the one hand, the encapsulation structure can protect metal NPs from growing larger. On the other hand, the coated N-doped graphene shells can stabilize the NPs and greatly reduce the leaching of cobalt for the catalyst. All in all, the structure of carbon-coated cobalt NPs is essential, which is directly related to the lifetime of CoO_x@CN.

The decreased activity of CoO_x@CN at the initial phase was primarily attributed to the cobalt leaching as mentioned above. Why the catalytic performance of the catalyst improved at the second stage? It sparked our curiosity. We speculated that the phenomenon was the result of the variation of the metal phase. In Figure 5, the diffraction peaks of Co_3O_4 and Co^0 were corroborated by XRD for the fresh catalyst. Specially, XRD patterns showed that Co_3O_4 NPs in

the CoO_x@CN were transformed into CoO after one use. What is more, only the diffraction peaks of Co^0 were recorded for the catalyst after 12 times use. This suggested that CoO may be mostly converted to Co^0 as the recycle progress. Density functional theory (DFT) calculations have demonstrated that Co^0 encapsulated by N-doped graphene layers can pleasingly make the inert graphene layers active in H_2 activation.[47] That is, the converted Co^0 can enormously promote the H_2 activation, thus improving the catalytic activity during the recycle despite existence of leaching. Along with the leaching of the active metal, a drop in performance of the catalyst was inevitable, corresponding to the decreased catalytic activity after the tenth recycle. To make it clear, we employed hydrogen temperature-programmed reduction (H_2-TPR) to investigate the reducibility of the NPs. Two obvious reduction peaks of Co_3O_4 were detected in CoO_x@CN, much lower than that of commercial Co_3O_4 (Figure S13), suggesting the Co_3O_4 NPs in CoO_x@CN was probable to be reduced with H_2. The H_2-TPR results concluded that Co_3O_4 in the hybrid CoO_x@CN can be gradually reduced to CoO and Co^0 at 120 ^oC and 3 MPa. Such a good stability could be ascribed to the following reasons: 1) The N-doped graphene layers protect the cobalt NPs from the aggregation and leaching; 2) the coated graphene layers greatly weaken the strong coordination between N-heterocycle and active metal NPs; 3) the CoO_x can be mostly converted to Co^0 under the reaction conditions, which can promote the H_2 activation and prolong the life of the catalyst.

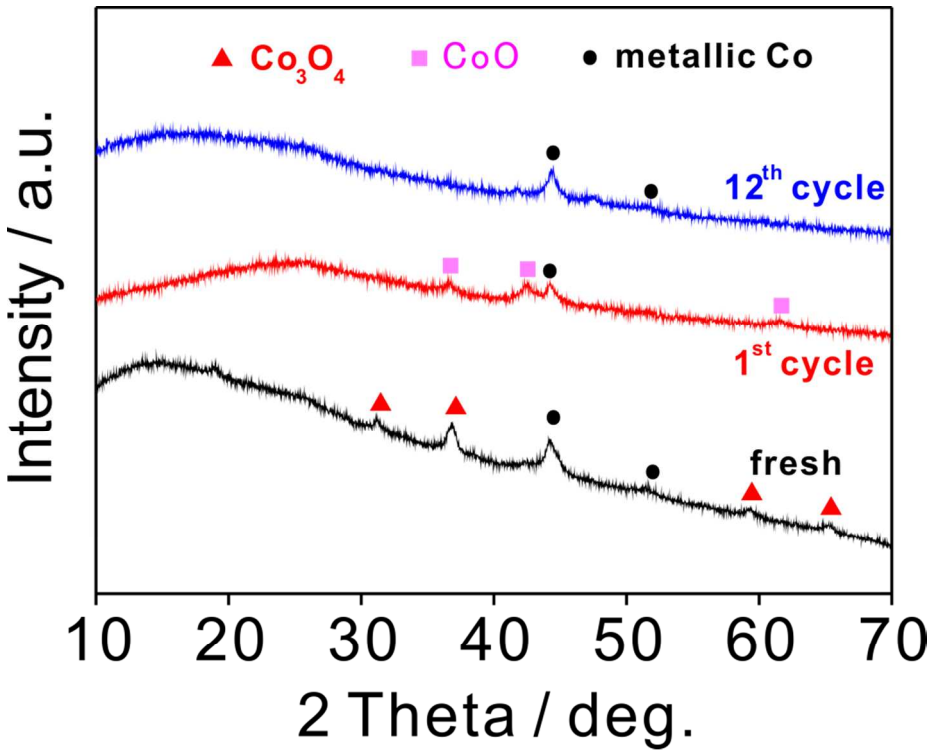

Figure 5. XRD patterns of CoO_x@CN after one use and 12 times use.

With the optimized reaction parameters in hand, the general scope of CoO_x@CN in the hydrogenation of quinoline compounds was investigated, including industrially and biologically relevant heteroarenes. Gratifyingly, the hydrogenation process appeared to be universally valid, and full conversions and essentially perfect chemoselectivity were observed for a series of *N*-heteroarenes, better than the reported works.[10] Quinolines compounds substituted with a methyl group at the 2-, 6- and 8- position could be readily transformed to the corresponding py-THQ, which were characterized by excellent conversions and selectivities (Table 4, entries 2-4). Notably, quinolines substituted by halogen were reduced efficiently to the corresponding halo-substituted py-THQ without any dehalogenation (Table 4, entries 5). What should be noted is the facile reduction of 8-hydroxyquinolines to biologically active 1,2,3,4-tetrahydro-8-hydroxyquinoline, which can inhibit leukotriene formation in macrophages

(Table 4, entry 6).[20] Also noteworthy is that other biologically important *N*-heteroarenes such as acridine, quinoxaline, and isoquinoline were also converted into the target products in high yields (Table 4, entries 7-9).

Table 4. Chemoselective hydrogenation of various substituted quinolones and N-heterocycles [a]

Entry	Substrate	Product	Time (h)	Conv. (%)[b]	Yield (%)[b]
1	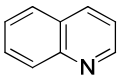	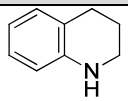	3	100	100 (95)
2	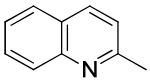	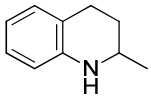	10	100	100 (94)
3	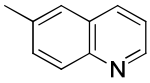	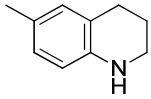	10	100	100 (95)
4	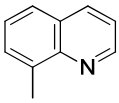	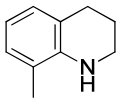	6	99	99 (95)
5[c]	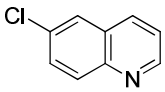	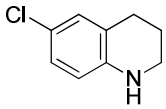	3	99	94
6[d]	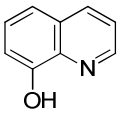	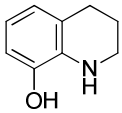	12	100	100 (89)
7	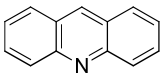	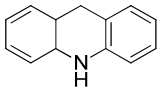	4	96	96 (88)
8	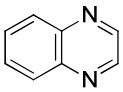	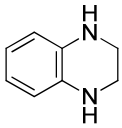	10	87	77 (65)
9	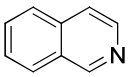	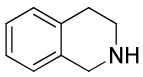	15	100	100 (92)

[a]Reaction conditions: substrate (0.5 mmol), CoO_x@CN (10mg), CH_3OH (5 mL), 3 MPa H_2, 120 °C. [b]Determined by GC (internal standard: n-dodecane), GC–MS and ^{1}H-NMR (Figure S14,15). Numbers in parentheses represent isolated yields. [c]110 °C. [d]CoO_x@CN (20mg), 140°C.

CONCLUSIONS

In summary, we have demonstrated that the Co-based hybrids featuring encapsulated Co NPs within the porous N-doped graphene layers served as catalysts with excellent catalytic activity and good stability for the chemoselective hydrogenation of *N*-heteroarenes. The considerable catalytic performance is attributed to the following reasons: 1) the encapsulation structure can enormously reduce the leaching of base metals and protect metal NPs from growing larger. 2) The large surface area and the mesoporous pores enable the easy approached catalytically active sites. 3) The better mixing effect. CoO_x@CN can mix the reactant in nano size and sufficiently contact with the reactant. 4) The coated N-doped carbon provides a layer of protection between N-heterocycle and active metal NPs, greatly weakening the strong coordination. The achieved success in the encapsulation of metal NPs within graphene layers pave the way for designing highly active and reusable heterogeneous catalysts for more challenging molecules.

EXPERIMENTAL SECTION

Preparation of Catalysts

GAH, melamine, $Co(OAc)_2{\cdot}4H_2O$, cobalt powder, Co_3O_4, Ru/C, Pd/C, and Pt/C were purchased from Aladdin. All chemicals used were analytical grade.

Synthesis of MO_x@CN (M = Co, Fe or Ni): 1 g GAH, 40 g melamine and a certain amount of metal salt (0.81 g $Co(OAc)_2{\cdot}4H_2O$, or 1.67 g $Fe(NO_3)_3{\cdot}9H_2O$, or 1.10 g $Ni(NO_3)_2{\cdot}6H_2O$) were thoroughly mixed. First, the resulting solids were placed into a crucible and heated up to 600 ^oC in 4 h, then it kept at 600 ^oC for 1 h. After that, we further rose the temperature to 800 ^oC in 2 h and maintained for another 1 h in N_2 flow. Finally, the catalysts were obtained when it cooled down to room temperature.

Synthesis of CoO_x NPs deposited to the outer surface of active carbon (AC) and nitrogen-doped carbon (CN): The catalysts CoO_x-AC and CoO_x-CN were prepared by wetness impregnation method: 0.58 g of $Co(OAc)_2 \cdot 4H_2O$ was first dissolved in 5 mL of deionized water; to this solution 0.5 g of support (AC or CN) was added. The resulting slurry was dried in an oil-bath at 80 ^oC overnight. Then the resulting solids were placed into a crucible and heated up to 600 ^oC in 4 h, then it kept at 600 ^oC for 1 h. After that, we further rose the temperature to 800 ^oC in 2 h and maintained for another 1 h in N_2 flow. Finally, the catalysts were obtained when it cooled down to room temperature.

Characterization Analyses

TEM experiments were conducted on a Hitachi H7700 instrument, operating at 100 kV. HRTEM images were taken on Tecnai G2 F30 S-Twin, working on 300 kV. The BET surface area and pore volume were measured by N_2 adsorption-desorption experiments with a Micromeritics ASAP 2020 HD88. Powder XRD measurements were carried out on Model D/tex-Ultima TV using Cu Ka radiation (1.54 Å). The sample was scanned in the 2 θ range from 10° and 80°. XPS characterization was performed on an ESCALAB MARK II spherical analyzer with an aluminum anode (Al 1486.6 eV) X-ray source. The Raman spectra were recorded on a Raman spectrometer (JY, HR 800) with a 514 nm laser. ICP-AES measurements were conducted on PerkinElmer Optima OES 8000. H_2-TPR was carried out on a FINESORB-3010 apparatus with a thermal conductivity detector (TCD).

Catalytic Applications in the hydrogenation reaction

The hydrogenation of quinoline was studied in a 50 mL stainless steel high-pressure batch reactor. Typically, quinoline (0.5mmol), the cobalt catalyst (CoO_x@CN, 10 mg) and the solvent

(5 mL) were loaded into the autoclave. First, the reactor was purged three times by pure H_2 to remove air. After that, the reactor was charged with 3 MPa H_2 and the reaction mixture was stirred 120 ^{o}C. The catalytic experiments were performed at agitation speed of 1500 rpm to rule out the external mass transfer limitation. After reaction finished, the reaction products were analyzed by gas chromatograph from Shimadzu with a Rtx-1071 column using n-dodecane as the internal standard, as well as by GC-MS (Agilent Technologies, GC 6890N, MS 5970) and ^{1}H-NMR. For the reuse of the catalyst, the hydrogenation of quinoline was conducted with 1mmol scale (1 mmol quinoline, 20 mg CoO_x@CN, and 10 mL methanol) at 120 ^{o}C and 3 MPa. After the reaction, CoO_x@CN was recycled by centrifugation or a magnet and then washed several times with ethanol. Finally, the recycled catalyst was dried overnight in an oven at 70 ^{o}C.

TOF = initial rate / (metal amount × time)

ASSOCIATED CONTENT

Supporting Information. Detailed characterizations of the CoO_x@CN, Raman spectra of the treated catalyst, GC-MS, ^{1}H-NMR results of the products and supplementary figures. This material is available free of charge via the Internet at http://pubs.acs.org.

AUTHOR INFORMATION

Corresponding Author

*Tel.: 86-571-88273551. Fax: +86-571-87951895. E-mail: chemwy@zju.edu.cn.

Notes

The authors declare no competing financial interest.

ACKNOWLEDGEMENT

Financial support from the National Natural Science Foundation of China (91534114, 21376208), the MOST (2016YFA0202900), the Zhejiang Provincial Natural Science Foundation for Distinguished Young Scholars of China (LR13B030001), the Fundamental Research Funds for the Central Universities (2016FZA3006), and the Partner Group Program of the Zhejiang University and the Max-Planck Society are greatly appreciated.

REFERENCES

(1) Bullock, R. M. *Science* **2013**, *342*, 1054-1055.
(2) Jagadeesh, R. V.; Surkus, A. E.; Junge, H.; Pohl, M. M.; Radnik, J.; Rabeah, J.; Huan, H. M.; Schunemann, V.; Bruckner, A.; Beller, M. *Science* **2013**, *342*, 1073-1076.
(3) Meffre, A.; Mehdaoui, B.; Connord, V.; Carrey, J.; Fazzini, P. F.; Lachaize, S.; Respaud, M.; Chaudret, B. *Nano Lett.* **2015**, *15*, 3241-3248.
(4) Westerhaus, F. A.; Jagadeesh, R. V.; Wienhofer, G.; Pohl, M. M.; Radnik, J.; Surkus, A. E.; Rabeah, J.; Junge, K.; Junge, H.; Nielsen, M.; Bruckner, A.; Beller, M. *Nat. Chem.* **2013**, *5*, 537-543.
(5) Chen, F.; Surkus, A.-E.; He, L.; Pohl, M.-M.; Radnik, J.; Topf, C.; Junge, K.; Beller, M. *J. Am. Chem. Soc.* **2015**, *137*, 11718-11724.
(6) Yao, Y.; Fu, Q.; Zhang, Y. Y.; Weng, X.; Li, H.; Chen, M.; Jin, L.; Dong, A.; Mu, R.; Jiang, P.; Liu, L.; Bluhm, H.; Liu, Z.; Zhang, S. B.; Bao, X. *Proc. Natl. Acad. Sci. U. S. A.* **2014**, *111*, 17023-17028.
(7) Czaplik, W. M.; Neudorfl, J.-M.; von Wangelin, A. J. *Green Chem.* **2007**, *9*, 1163-1165.
(8) Liu, C.; Rong, Z.; Sun, Z.; Wang, Y.; Du, W.; Wang, Y.; Lu, L. *RSC Adv.* **2013**, *3*, 23984-23988.
(9) Friedfeld, M. R.; Shevlin, M.; Hoyt, J. M.; Krska, S. W.; Tudge, M. T.; Chirik, P. J. *Science* **2013**, *342*, 1076-1080.
(10) Shylesh, S.; Schünemann, V.; Thiel, W. R. *Angew. Chem. Int. Ed.* **2010**, *49*, 3428-3459.
(11) Lee, J.; Jackson, D. H. K.; Li, T.; Winans, R. E.; Dumesic, J. A.; Kuech, T. F.; Huber, G. W. *Energy Environ. Sci* **2014**, *7*, 1657-1660.
(12) Rahi, R.; Fang, M.; Ahmed, A.; Sanchez-Delgado, R. A. *Dalton Trans.* **2012**, *41*, 14490-14497.
(13) Gong, Y.; Zhang, P.; Xu, X.; Li, Y.; Li, H.; Wang, Y. *J. Catal.* **2013**, *297*, 272-280.
(14) Hakki, A.; Dillert, R.; Bahnemann, D. W. *ACS Catal.* **2013**, *3*, 565-572.
(15) Karakulina, A.; Gopakumar, A.; Akçok, İ.; Roulier, B. L.; LaGrange, T.; Katsyuba, S. A.; Das, S.; Dyson, P. J. *Angew. Chem. Int. Ed.* **2016**, *55*, 292-296.
(16) Rosales, M.; Bastidas, L.; González, B.; Vallejo, R.; Baricelli, P. *Catal. Lett.* **2011**, *141*, 1305-1310.

(17) Wang, W.-B.; Lu, S.-M.; Yang, P.-Y.; Han, X.-W.; Zhou, Y.-G. *J. Am. Chem. Soc.* **2003**, *125*, 10536-10537.
(18) Dobereiner, G. E.; Nova, A.; Schley, N. D.; Hazari, N.; Miller, S. J.; Eisenstein, O.; Crabtree, R. H. *J. Am. Chem. Soc.* **2011**, *133*, 7547-7562.
(19) Wang, T.; Zhuo, L.-G.; Li, Z.; Chen, F.; Ding, Z.; He, Y.; Fan, Q.-H.; Xiang, J.; Yu, Z.-X.; Chan, A. S. C. *J. Am. Chem. Soc.* **2011**, *133*, 9878-9891.
(20) Ren, D.; He, L.; Yu, L.; Ding, R.-S.; Liu, Y.-M.; Cao, Y.; He, H.-Y.; Fan, K.-N. *J. Am. Chem. Soc.* **2012**, *134*, 17592-17598.
(21) Yan, M.; Jin, T.; Chen, Q.; Ho, H. E.; Fujita, T.; Chen, L.-Y.; Bao, M.; Chen, M.-W.; Asao, N.; Yamamoto, Y. *Org. Lett.* **2013**, *15*, 1484-1487.
(22) Tao, L.; Zhang, Q.; Li, S.-S.; Liu, X.; Liu, Y.-M.; Cao, Y. *Adv. Synth. Catal.* **2015**, *357*, 753-760.
(23) Mao, H.; Ma, J.; Liao, Y.; Zhao, S.; Liao, X. *Catal. Sci. Technol.* **2013**, *3*, 1612-1617.
(24) Dell'Anna, M. M.; Capodiferro, V. F.; Mali, M.; Manno, D.; Cotugno, P.; Monopoli, A.; Mastrorilli, P. *Appl. Catal. A- Gen.* **2014**, *481*, 89-95.
(25) Ge, D.; Hu, L.; Wang, J.; Li, X.; Qi, F.; Lu, J.; Cao, X.; Gu, H. *Chemcatchem* **2013**, *5*, 2183-2186.
(26) Fang, M.; Machalaba, N.; Sanchez-Delgado, R. A. *Dalton Trans.* **2011**, *40*, 10621-10632.
(27) Fang, M.; Sanchez-Delgado, R. A. *J. Catal.* **2014**, *311*, 357-368.
(28) Zhang, L.; Wang, X.; Xue, Y.; Zeng, X.; Chen, H.; Li, R.; Wang, S. *Catal. Sci. Technol.* **2014**, *4*, 1939-1948.
(29) Zhu, D.; Jiang, H.; Zhang, L.; Zheng, X.; Fu, H.; Yuan, M.; Chen, H.; Li, R. *Chemcatchem* **2014**, *6*, 2954-2960.
(30) Bianchini, C.; Dal Santo, V.; Meli, A.; Moneti, S.; Moreno, M.; Oberhauser, W.; Psaro, R.; Sordelli, L.; Vizza, F. *J. Catal.* **2003**, *213*, 47-62.
(31) Barbaro, P.; Gonsalvi, L.; Guerriero, A.; Liguori, F. *Green Chem.* **2012**, *14*, 3211-3219.
(32) Fan, G.-Y.; Wu, J. *Catal. Commun.* **2013**, *31*, 81-85.
(33) Sánchez, A.; Fang, M.; Ahmed, A.; Sánchez-Delgado, R. A. *Appl. Catal. A- Gen.* **2014**, *477*, 117-124.
(34) Niu, M.; Wang, Y.; Chen, P.; Du, D.; Jiang, J.; Jin, Z. *Catal. Sci. Technol.* **2015**, *5*, 4746-4749.
(35) Beckers, N. A.; Huynh, S.; Zhang, X.; Luber, E. J.; Buriak, J. M. *ACS Catal.* **2012**, *2*, 1524-1534.
(36) Corma, A.; Serna, P.; Concepción, P.; Calvino, J. J. *J. Am. Chem. Soc.* **2008**, *130*, 8748-8753.
(37) Wang, D.-S.; Chen, Q.-A.; Lu, S.-M.; Zhou, Y.-G. *Chem. Rev.* **2012**, *112*, 2557-2590.
(38) Dell'Anna, M. M.; Capodiferro, V. F.; Mali, M.; Manno, D.; Cotugno, P.; Monopoli, A.; Mastrorilli, P. *Appl. Catal., A* **2014**, *481*, 89-95.
(39) Mao, H.; Peng, S.; Yu, H.; Chen, J.; Zhao, S.; Huo, F. *J. Mater. Chem. A* **2014**, *2*, 5847-5851.
(40) Erokhin, A. V.; Lokteva, E. S.; Yermakov, A. Y.; Boukhvalov, D. W.; Maslakov, K. I.; Golubina, E. V.; Uimin, M. A. *Carbon* **2014**, *74*, 291-301.
(41) Liu, R.; Mahurin, S. M.; Li, C.; Unocic, R. R.; Idrobo, J. C.; Gao, H. J.; Pennycook, S. J.; Dai, S. *Angew. Chem., Int. Ed.* **2011**, *50*, 6799-6802.
(42) Gao, Z.; Dong, M.; Wang, G.; Sheng, P.; Wu, Z.; Yang, H.; Zhang, B.; Wang, G.; Wang, J.; Qin, Y. *Angew. Chem., Int. Ed.* **2015**, *54*, 9006-9010.

(43) Chen, L.; Chen, H.; Luque, R.; Li, Y. *Chem. Sci.* **2014**, *5*, 3708-3714.
(44) Tian, H.; Li, X.; Zeng, L.; Gong, J. *ACS Catal.* **2015**, *5*, 4959-4977.
(45) Li, X.-H.; Antonietti, M. *Angew. Chem. Int. Ed.* **2013**, *52*, 4572-4576.
(46) Wang, J.; Wei, Z.; Gong, Y.; Wang, S.; Su, D.; Han, C.; Li, H.; Wang, Y. *Chem. Commun.* **2015**, *51*, 12859-12862.
(47) Wei, Z.; Wang, J.; Mao, S.; Su, D.; Jin, H.; Wang, Y.; Xu, F.; Li, H.; Wang, Y. *ACS Catal.* **2015**, *5*, 4783-4789.
(48) Yang, S.; Cao, C.; Sun, Y.; Huang, P.; Wei, F.; Song, W. *Angew. Chem., Int. Ed.* **2015**, *54*, 2661-2664.
(49) Rao, A. M.; Eklund, P. C.; Bandow, S.; Thess, A.; Smalley, R. E. *Nature* **1997**, *388*, 257-259.
(50) Shin, H.-J.; Choi, W. M.; Choi, D.; Han, G. H.; Yoon, S.-M.; Park, H.-K.; Kim, S.-W.; Jin, Y. W.; Lee, S. Y.; Kim, J. M.; Choi, J.-Y.; Lee, Y. H. *J. Am. Chem. Soc.* **2010**, *132*, 15603-15609.
(51) Shin, H.-J.; Kim, S. M.; Yoon, S.-M.; Benayad, A.; Kim, K. K.; Kim, S. J.; Park, H. K.; Choi, J.-Y.; Lee, Y. H. *J. Am. Chem. Soc.* **2008**, *130*, 2062-2066.
(52) Tang, M.; Mao, S.; Li, M.; Wei, Z.; Xu, F.; Li, H.; Wang, Y. *ACS Catal.* **2015**, *5*, 3100-3107.
(53) Casanova, O.; Iborra, S.; Corma, A. *J. Catal.* **2009**, *265*, 109-116.
(54) Sun, B.; Khan, F.-A.; Vallat, A.; Süss-Fink, G. *Appl. Catal. A- Gen.* **2013**, *467*, 310-314.
(55) Xu, X.; Tang, M.; Li, M.; Li, H.; Wang, Y. *ACS Catal.* **2014**, *4*, 3132-3135.